IL NUOVO CIMENTO **48 C** (2025) 52
DOI 10.1393/ncc/i2025-25052-y

Colloquia: IWM-EC 2024

Nuclear EoS with finite range interaction and the Constrained Dynamics

M. Papa

INFN, Sezione di Catania - Catania, Italy

received 26 November 2024

Summary. — The effects of the many-body correlations with respect to a MF description characterizing the Constrained Molecular Dynamics are discussed in the case of finite and zero range effective microscopic interactions. In particular, for the system ^{64}Ni+^{48}Ca fusion-fission cross-sections, IMF production and transversal flow have been evaluated in the framework of the CoMD model at different incident energies. The results obtained significantly depend on whether or not the effects of the above-mentioned correlations are taken into account in the corresponding EoS.

1. – Introduction

The description of many-body systems is one of the most difficult problems in nuclear physics due to their complexity being quantum objects described by a large number of degrees of freedom. In particular, the heavy ion collisions (HIC) at energy well above the mutual Coulomb barriers are usually described through semi-classical approaches based on the mean-field (MF) approximation or quantum molecular dynamics approaches (QMD) [1]. These last describe the single particle wave functions by means of well localized wave-packets (WPs) with fixed widths. In this way many-body correlations are produced which lead to the spontaneous formation of clusters. In these semi-classical approaches the effective interaction plays obviously a key role, and in many cases it just represents the main subject of investigation. In several cases MF and molecular dynamics approaches [1] share the same microscopic effective interactions. From a general point of view, it can be expected that the typical and explicit two or many-body correlations of QMD-like approaches could instead play a role in many-body quantities as for the total energy. At what extent these specific correlations may affect the many-body functional (EDF) related to the total energy in the case of infinite nuclear matter (NM) was discussed in some detail in refs. [2,3]. In particular, in this contribution, we aim to illustrate how these correlations influence some common observables studied in HIC at the Fermi energies, such as fusion-fission and intermediate mass fragment (IMF) production.

In the following section the topic is introduced by specifying the microscopic effective interaction used and briefly discussing the procedure adopted to obtain the set of parameters describing a reference Equation of State (EoS) around the saturation density. In the other sections proceeding to finite systems the results of calculation concerning the ^{64}Ni+^{48}Ca collision at different energies are shown. In particular, for the case of finite and zero range interaction (ZR) the comparison of different reaction mechanisms and the nucleon transverse flow for central/semi-central collisions is illustrated. To understand to what extent the correlations produced by the model can affect the above observables, comparisons using the set of parameter values obtained in the MF scheme are also shown.

2. – The microscopic effective interaction

In the following we will refer to an example of EoS characterized by some properties at the saturation density at zero temperature that we choose as reference. Equilibrium density $\rho_0 = 0.165\,\mathrm{fm}^{-3}$, associated binding energy $E(\rho_0) = -16\,\mathrm{MeV}$, incompressibility $K(\rho_0) = 240\,\mathrm{MeV}$, symmetry energy $E_{sym} = 30\,\mathrm{MeV}$, an effective pairing energy (it includes the spin-dependent one produced through the exchange terms [2]) equal to $-2\,\mathrm{MeV}$ per nucleon at the saturation density in finite systems (around mass 100). Moreover, the functional will correspond in the MF limit to a relative effective mass $m^*_r = 0.67$, and neutron-proton effective mass splitting $m^*_{rn} - m^*_{rp} = 0.4\beta$. Different values of the slope parameter associated to the symmetry energy $L = 3\rho_0(\frac{\mathrm{d}E_{sym}}{\mathrm{d}\rho})_{\rho_0}$ have been considered changing in the range 55–105 MeV as suggested from different investigations (see as an example [4]). The total microscopic interaction, inspired from the Gogny interaction, will be the sum of two and three body terms with zero and finite range $\mu = 1.1$ fm. The finite range is modelled according to Gaussian factors. Finally, a further term corresponding to eq. (1e) in [2] represents a zero range spin-spin interaction. As explained in the following section, this contribution is necessary to reproduce an effective "pairing" energy of about $-2\,\mathrm{MeV}$ at the ground state for finite system with mass around 100 (see also the following section). At the same time, in box calculations, this further contribution is able to locally produce small values of the average total spin at the stationary conditions. The introduction of this term produces a further contribution to the symmetry energy.

3. – The effective interaction

Starting from the microscopic interaction, the expression of the effective interaction as a function of the density can be obtained in the MF approximation by evaluating the associated matrix elements using 2-body wave functions constructed with plane-waves in a large volume V, $\Phi = \frac{1}{\sqrt{V}} e^{i\mathbf{kr}}$. The zero range interactions will give rise to the usual terms proportional to powers of the density. The finite range interaction will give rise to a momentum-dependent part because of the underlying Slater determinant structure of the 2-body wave function for the identical particles. Contrary to the Gogny case, it has been supposed, according to the several experimental evidences collected on the isospin symmetry breaking in nuclei [5], that the neutron and proton are different kind of particles. Therefore in the present approach neutron-proton couples do not generate exchange terms and the related momentum-dependent interaction. This condition, as noted in the previous paragraph, required the introduction of the term associated with eq. (1e) of ref. [2] in order to produce the desired effective mass and effective "pairing".

In the following as an example we write the two-body exchange contribution:

$$\Delta E_2^{ex}(\mathbf{k}_i,\mathbf{k}_j) = -\frac{P_2}{V}(\sqrt{\pi}\mu)^3 e^{-\mu^2(\mathbf{k}_i-\mathbf{k}_j)^2/4}. \tag{1}$$

The non-locality of the effective interactions produces corrective factors to the in medium nucleon kinetic energy formally represented through a density-dependent nucleon effective mass m^*. In the case of the CoMD model the first step is just to substitute the plane-waves convolution with the wave packets $\Phi = \frac{1}{(2\pi\sigma_r^2)^{3/4}} e^{-\frac{(\mathbf{r}-\mathbf{r}_{0,i})^2}{4\sigma_r^2}+i\mathbf{k}_{0,i}\mathbf{r}}$. As an example, the corresponding momentum-dependent (MDI) 2-body contribution will be

$$E_2^{i,j,MDI} = -\frac{P_2}{8\sigma_r^3}\xi^3 \times e^{-\frac{1}{4}[\frac{(\mathbf{r}_{0,i}-\mathbf{r}_{0,j})^2}{\sigma_r^2}+\xi^2(\mathbf{k}_1-\mathbf{k}_1)^2]}(\delta_{\tau_i-\tau_j}\delta_{s_i-s_j}). \tag{2}$$

With a modified width $\frac{1}{\xi^2} = \frac{1}{4\sigma_r^2} + \frac{1}{\mu^2}$. While the Gaussian width of the related direct contribution will be $\lambda^2 = 4\sigma_r^2 + \mu^2$. The differences in the arguments of the exponentials appearing in eqs. (1) and (2) should be noted. They are the principal reasons together with the Pauli constraint for the existence of typical correlations in the molecular dynamics approach not present in the MF one [2] .

In the framework of the MF approximation, all the quantities characterizing the reference functional can be obtained in a relatively simple way by solving a linear system with the strength parameters as unknown quantities. In the case of CoMD calculations the nuclear matter is simulated by means of box calculations with periodic boundary conditions. The functionals associated to the different combination of overlap integrals at the different densities are evaluated numerically from the simulations. This is obtained after the cooling/warming procedures associated to the Pauli constraint. From the average overlaps (on different microscopic configurations) at different densities it is possible to obtain the linear system for the strength parameters whose solution will produce the reference EoS.

4. – Finite systems

4˙1. *Finite range interaction and reaction mechanisms.* – In this section the above-discussed effective interaction in CoMD calculations is used to study, as an example, the ^{64}Ni+^{48}Ca collision at different incident energies. This system has been also widely experimentally investigated (see ref. [6] as an example). A comparison between reaction mechanisms produced using a ZR effective interaction ($m_r^* = 1$) with parameter values modified for the CoMD correlations (ZR-MD) and the above-described finite range interaction (MDI-MD) will be illustrated in the next section. In the same section we also add the interesting comparison with the case of the MDI with parameters obtained in the MF scheme (MDI-MF). This comparison in fact allows to estimate how the typical MD correlation affects the dynamics of the heavy collisions.

4˙2. *The interaction and the "ground state" configuration.* – Moving on to finite systems the surface properties acquire a relevant role that cannot be described in the limit of an infinite NM. Therefore a correction term E_s is usually introduced in the total energy of A nucleons through the following expression: $E_s = \frac{C_s'}{2}(4\pi\sigma_r^2)^{1.5}\sum_{i=1,A}\nabla_i^2 S_v^i$.

In CoMD for finite systems, this correction term is fixed through a warming-cooling procedure applied to the microscopic configuration of the system under study and driven through the Pauli constraint. A stabilization stage follows. In the present calculations, the process is stopped when the system reaches the given binding energy, the root-mean-radius, average kinetic energy, in a stable way (within 8% of the requested values) for a time interval of about 300 fm/c. For the three mentioned interactions MDI-MD, ZR-MD and MDI-MF good "ground state" properties are reached by setting $C_s = -11\,\mathrm{MeV{\cdot}fm^2}$, $C_s = 3\,\mathrm{MeV{\cdot}fm^2}$ and $C_s = -7\,\mathrm{MeV{\cdot}fm^2}$, respectively. The strength parameters of the effective interaction have been fixed to the values reported in the first row of table 1, table 2 and appendix B of ref. [2] for the cases MDI-MF, MDI-MD and ZR-MD, respectively.

4˙3. *Selection and comparison of the reaction mechanisms and transverse flow.* – Collisions in a wide range of impact parameters up to the "grazing" collision have been calculated with the CoMD model to identify different reaction mechanisms. In fig. 1 for the case ZR-MD the bi-dimensional plot Z-V_p for the collision ^{64}Ni+^{48}Ca at different incident energy is shown. Z represents the charge of the fragment formed after a maximum time of 350 fm/c. V_p represents the velocity of the produced fragments in the laboratory frame along the beam direction. Fragments are identified with a minimum-spanning-tree method. The figures refer to an impact parameter range b = 0–10.5 fm. In order to test the interactions, the present work will focus on the dynamics of processes producing fusion-incomplete fusion residues, fission and intermediate mass fragments in the mid-rapidity region in central/semi-central collisions. The aforementioned processes are well localized and almost exclusively selected in the range of impact parameters 0–5 fm (the bumps corresponding to the bynary processes are substantially absent).

In this case the fragments in the mid-rapidity region are mainly produced through the formation of one intermediate system in which the largest changes of density are produced. Furthermore, the primary source is formed by target and projectile nucleons having on average a relative velocity directly established through the beam energy (participant zone). Therefore we think that the aforementioned processes are better suited to discuss the behaviours of the interaction as a function of the incident energy. In particular in fig. 1 the upper rectangles define the region where the fusion/incomplete fusion residues have been integrated. Inside the lower rectangles we show the cross-section for production of Intermediate Mass Fragments (IMF) which are defined as fragments having charge $Z = 3{-}12$. In the same region of velocity a kind of "fission" of the hot residues is associated to the production, in the same event, of two fragments 1 and 2 heavier than the nitrogen and having comparable charges (with the associate ratio of the charges $Z1/Z2$ greater than 0.8 and $Z2$ larger than or at most equal to $Z1$). For the energies not shown in the figure the velocity ranges have been scaled proportionally to the center of mass (c.m.) velocity. As observed before, in the present work the quantitative analysis will be focused on the impact parameter range b = 0–5 fm where the above mechanisms are well localized.

In the interval of considered impact parameters and for the energy interval 10–50 AMeV the mechanism is characterized by the production of a bump in the Z-V_p plots centred around the c.m. velocity. In addition to the IMF production, heavy residues can be identified having charge Z higher than 20. This happens for both the MDI and the ZR cases. In these calculations due to the impact parameter selection the binary mechanisms are absent. In fig. 2 for the MDI-MD and ZR-MD cases, the integrated cross-section for the production of heavy residues (as defined above) is shown as a function of the incident energy. They are represented by black squares and blue dots, respectively. In the inset

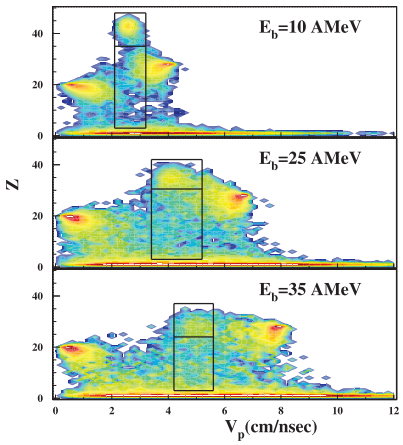

Fig. 1. – For the collisions ^{64}Ni+^{48}Ca (ZR-MD case), for the impact parameter range $b = 0$–10.5 fm, the produced fragment charges Z *vs.* the laboratory velocities V_p along the beam direction are plotted for different incident energies. The rectangles define the regions where the different reaction mechanisms are integrated (see text) (color online).

panel the associated fission probabilities estimated as $P_f = \frac{N_{fis}}{N_{fus}+N_{fis}}$ are also plotted. In the above expression N_{fis} and N_{fus} indicate the selected number of events for fusion and fission, respectively.

Within this energy range, the globally more repulsive character of the finite range interaction case (MDI-MD) gives rise to a more probable disassembly of the hot compound. It in fact produces a lower cross-section for the formation of hot residues and an enhanced "fission" probability for E_{inc} at 25 and 35 AMeV. This more repulsive

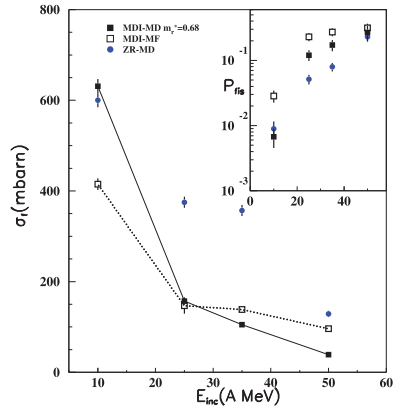

Fig. 2. – As a function of the incident energy E_{inc} for the ^{64}Ni+^{48}Ca collision and for an impact parameter range $b = 0$–5 fm the evaluated cross-section associated to the formation of an heavy residue is plotted. The blue dots and the black square symbols refer to the ZR-MD and MDI-MD cases, respectively. The open squares represent the results for the MDI-MF case. In the inset the fission probabilities are also shown. The lines joining the points MDI-MD and MDI-MF are plotted to simplify the comparison between the two cases. (color online).

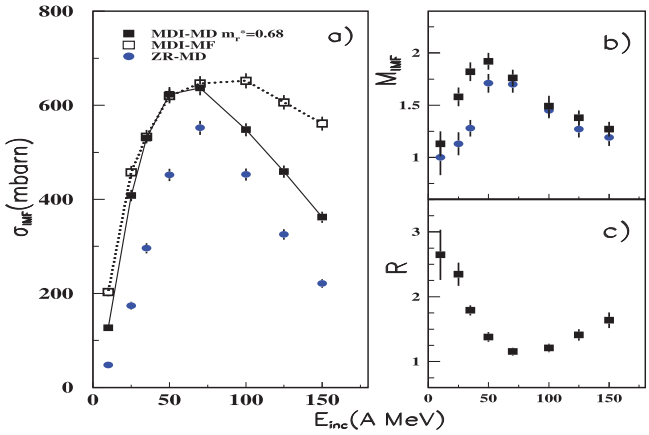

Fig. 3. – For the system ^{64}Ni+^{48}Ca, in the impact parameters range b = 0–5 fm: panel (a) shows for the MDI-MD, MDI-MF, ZR-MD cases the cross-section for the production of at least one IMF as a function of the incident energy E_{inc}, panel (b) shows the associated multiplicity MDI-MD and ZR-MD, panel (c) shows the ratio $R = \sigma_{IMF}^{MDI-MD}/\sigma_{IMF}^{ZR-MD}$. The lines joining the points MDI-MD and MDI-MF are plotted to simplify the comparison between the two cases (color online).

character of the MDI-MD is also confirmed through the production of an higher rate of IMF. This is shown in fig. 3 where the cross-sections for producing at least one IMF in the mid-rapidity region and the related multiplicity are plotted in panels (a) and (b). We note that in both cases the rates of IMF have a maximum around 70 AMeV. The further increase of the energy produces disassembly processes with an increasing fraction of light particles with charge Z less than 3. This produces a lowering of the IMF rate in both cases.

In both figures the open square symbols represent instead the cross-sections for the case MDI-MF. The lines joining the points are plotted to simplify the comparison with the MDI-MD case. From this comparison it can be clearly observed how the corrections on the values of strength parameters due to the discussed MD correlations can sensitively affect the studied quantities.

Going back to the earlier comparisons MDI-MD, ZR-MD, in panel (c) the ratio $R = \sigma_{IMF}^{MDI-MD}/\sigma_{IMF}^{ZR-MD}$ associated to the IMF production is shown. The ratio R in this first part decreases with the energy.

In the analysed results at 100 AMeV and for the ZR case a small bump at velocity much higher than the c.m. one appears in the Z-V_p correlation plot (corresponding to $b \simeq 5$ fm). This hint of bump could be associated with the onset of a precursor mechanism for the production of projectile-like fragments. This bump is also present for the MDI-MD fm case but it is less pronounced. Therefore, the presence of this other mechanism produces around the c.m. velocity a larger depletion in the Z-V_p plot for the ZR-MD case with respect to the MDI-MD one and justifies the increasing behaviour of the ratio R shown in fig. 3(c) from 100 up to 150 AMeV.

The global repulsive action associated to the finite range interaction strongly affects also the nucleon transverse flow as shown in fig. 4. As an example for b = 3 fm, it produces the disappearance of the balance energy (which is seen for the ZR-MD case) with positive slopes in the explored energy range. In the upper energy limits the slopes

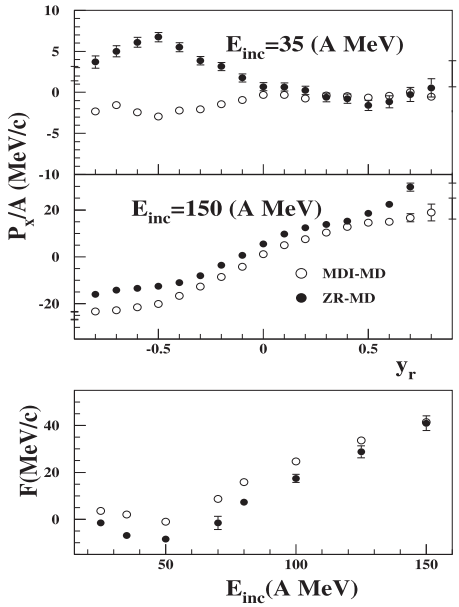

Fig. 4. – In the two upper panels, for the zero and the finite range interction (MDI) the average transverse momentum per nucleon ($b = 3$ fm) is plotted as a function of the c.m. reduced rapidity. In the bottom panel the slope parameters as a function of the incident energy are also shown.

for the two cases become comparable being more affected by the nucleon-nucleon collision rate.

Finally we observe that both the fast decreasing trend of the ratio R in the first 70 AMeV (corresponding to about 35 AMeV of relative motion) and the behaviour of the transverse flow slopes as functions of the beam energy could be interpreted through the existence of a characteristic relative kinetic energy per nucleon $E \simeq \frac{\hbar^2}{2m_0}\frac{2}{\xi^2}$ beyond which the momentum-dependent effects related to the finite range, in the pre-equilibrium stage of central/semi-central collisions are attenuated. Here $\hbar\frac{\sqrt{2}}{\xi}$ establishes the characteristic width of the MDI (see ref. [2]).

4˙4. *Conclusive remark.* – In this work, starting from some reference EoS properties at the saturation density, the effects of the finite range interaction as compared to the case of a zero range interaction for the system ^{64}Ni+^{48}Ca have been studied in semi-central collision at different energies by means of the CoMD model. Furthermore, for the same system the effects of the many-body correlations in the EoS obtained in the model (as compared to a MF approach) in fusion-like cross-section fission probability and IMF production in central collisions were found to be non-negligible. Finally, it is worth noting that even if the obtained numerical results are strictly valid for the specific model calculations, the rather general feature of the discussed correlations that are associated to the wave-packets dynamics and to the Pauli principle could give a wider meaning to the the comparisons illustrated in this work.

REFERENCES

[1] Wolter H. *et al.*, *Prog. Part. Nucl. Phys.*, **125** (2022) 103962 and references therein.
[2] Papa M., *Nucl. Phys. A*, **1041** (2024) 122780, and references therein.
[3] Papa M., Maruyama T. and Bonasera A., *Phys. Rev. C*, **64** (2001) 024612.
[4] Tsang M. B. *et al.*, *Phys. Rev. C*, **86** (2012) 015803.
[5] Sheikh J. A., Rouoof S. P., Ali R. N., Rather N., Sarma C. and Srivastava P. C., *Symmetry*, **16** (2024) 745 and references therein.
[6] Chun-Wang Ma *et al.*, *Chin. Phys. Lett.*, **29** (2012) 062101.